Damage of additively manufactured polymer materials: experimental and probabilistic analysis

Hachimi Taoufik, Ait Hmazi Fouad, Majid Fatima
Laboratory of Nuclear, Atomic, Molecular, Mechanical and Energetic Physics, University Chouaib Doukkali, El Jadida, Morocco
hachtaoufik@gmail.com, https://orcid.org/0000-0002-3567-8511
aithmazi.f@ucd.ac.ma, https://orcid.org/0009-0009-6919-5540
majidfatima9@gmail.com, https://orcid.org/0000-0001-8909-8232

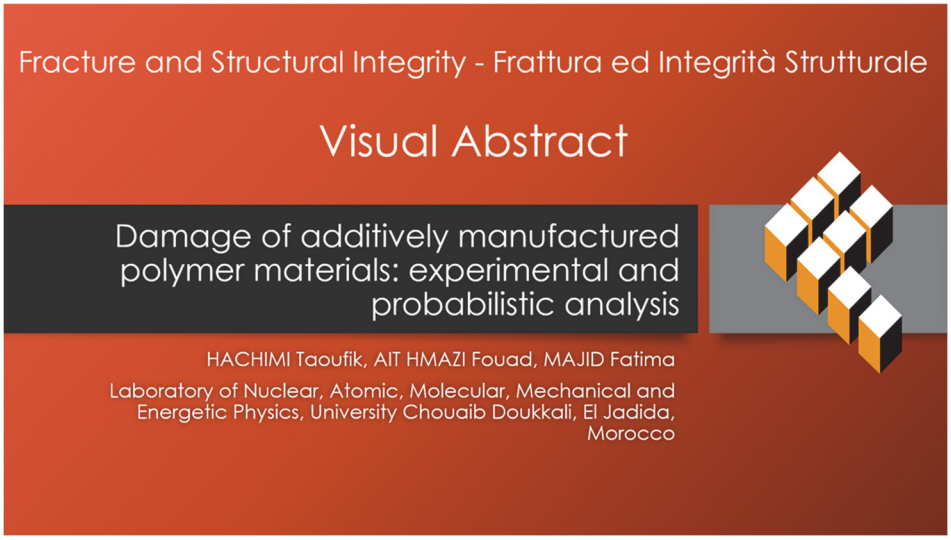

Citation: Taoufik, H., Fouad, A. H., Fatima, M., Damage of additively manufactured polymer materials: experimental and probabilistic analysis, Fracture and Structural Integrity, 73 (2025) 236-255.

Received: 11.05.2025
Accepted: 06.06.2025
Published: 11.06.2025
Issue: 07.2025

KEYWORDS. Damage analysis, Reliability analysis, 3D materials, Fused filament fabrication, Crack length.

INTRODUCTION

In recent years, three-dimensional (3D) printing, also known as additive manufacturing, has ushered in a disruptive period across a wide range of industries.[1,24,27] This ground-breaking technique enables the production of complex and personalized structures with remarkable precision, bringing enormous potential and difficulties in material science and engineering[18,26,33].

Crack propagation in 3D printed polymer components can significantly impact their mechanical properties and performance. The orientation of the raster angle during printing plays a crucial role in determining crack propagation behavior and mechanical characteristics [6,17]. Additionally, several studies have shown that as the specimen diameter decreases, the upper yield strength, lower yield strength, and plastic extension strength of miniaturized specimens decrease, while the elongation after fracture decreases as well [7,31,34]. Notch geometries during tensile tests play a significant role in determining the strain state, with optimization techniques used to enhance the Plane Strain State Index and Homogeneity Index [3]. Additionally, Koščo, T. [10] focuses on the problem of strain measurement on notched specimens, especially on

sharp notches (notches with small minimum radius) by using the digital image correlation method. Furthermore, in this article, an approximate method for calculating elastic-plastic stresses and strains on the surface of notched samples was proposed by Lutovinov et al. [13] based on the Abdel-Karim-Ohno cyclic plasticity model.

The damage evolution of 3D printing of polymers is a complex process influenced by various factors such as temperature, layer adhesion, cyclic loading, and material properties. Temperature variations can lead to changes in material strength [15,23,28]. Additionally, the lack of adherence between layers can significantly reduce the global resistance of printed materials, leading to delamination effects and crack growth [22]. Cyclic loading can result in the accumulation of plastic strain, affecting the ultimate strength and strain at break of the printed specimens [2]. Moreover, the interfacial bond between deposited layers plays a crucial role, with cyclic loading causing only a negligible detrimental effect on the ultimate tensile strength, making 3D-printed components suitable for applications exposed to cyclic loading [19].

Several studies collectively underscore the need for a comprehensive understanding of the factors influencing damage evolution in 3D printed polymers[5,16,21,29].

Guessasma highlights the role of process-induced anisotropy, with printing orientation affecting damage development in ABS polymer under compression [4]. Majid further explores this, focusing on the delamination effect and its impact on mechanical behavior, with a particular emphasis on the reduction in global resistance due to lack of adherence [15]. Moetazedian adds to this by examining the effect of the environment and cyclic loading on the damage accumulation in 3D printed PLA specimens, finding that cyclic loading can lead to a decrease in ultimate strength and strain at break and that the presence of water can plasticize the polymer, increasing strain at fracture[20]. Vanaei et al. [30] present an experimental analysis of the multi-scale damage and fatigue behavior of PLA manufactured by FDM, focusing on the influence of extruder temperature, loading parameters, and manufacturing orientation on mechanical properties and fatigue lifetime.

Majid and Elghorba introduced a new approach for failure analysis and prediction, identified critical life fraction and groove depth for understanding stages of damage, and developed simplified models for damage assessment based on static tests [14]. Cózar and Penumakala proposed a 3D elastoplastic damage model for composite materials, capturing plastic deformation and failure mechanisms [2,25]. Liu and Yang [12] experimentally investigate the influence of cyclic creep accumulation rate on the damage evolution of MDYB-3 polymethyl methacrylate (PMMA), observing that the cyclic creep accumulation rate, cyclic creep strain growth speed, and relaxed modulus degradation rate are factors that influencing damage evolution in 3D printing polymer. Lach et al. [11] saw that Building orientation, not printing speed, significantly influences damage evolution in 3D printed thermoplastic polymers. The 45°/45° orientation exhibits higher toughness due to mode II portions during fracture. (Zhang and Dong [32] show that the branch inclination angle of the kinked fissure is an important factor affecting the crack's initial position, and the evolution of the strain field during the damage process of the sample can better reflect the cracking law of the internal fissures. Jia et al [9] show that the damage evolution of 3D printing polymers is influenced by impact forces causing defects like cavities. Fast self-healing using dynamic urea bonds and direct recycling enhances material durability. The dynamic damage evolution for PP/PA blends with different compatibilizers is studied in high strain rates from two different approaches, namely by determining the unloading elastic modulus of the specimen that experienced impact deformation and by combining the split Hopkinson pressure bar (SHPB) experimental technique with the back-propagation (BP) neural network. Jayaraman discusses the development of damage modes in polymer composite laminates, the influence of loading conditions on their evolution, and the importance of a comprehensive review in this area for designers and researchers[8].

The theme elaborated in this article is the study of the mechanical behavior of different specimens printed by the FDM process, which focuses on the mechanical behavior of PLA material in different orientations. The study of fracture propagation is an important aspect of this subject since it has a significant impact on the structural integrity and reliability of 3D-printed components. In the realm of 3D printing, the layer-by-layer additive manufacturing approach introduces distinctive challenges due to the inherent anisotropic properties arising from the sequential deposition of material. This anisotropy can significantly influence crack propagation behavior, making it imperative to explore and comprehend the intricacies of crack initiation and growth in 3D-printed materials. This introduction digs into the complex interaction between 3D printing, crack propagation, damage evolution, and the analytical determination of Weibull parameters through knowledge of the complex phenomena related to crack growth and damage assessment in these materials.

MATERIAL SELECTION

Knowledge of the mechanical behavior of components is essential to predict their service life to avoid any fatal failure in service. Our study, therefore, analyzes the reliability of artificially damaged structures. Thus, to understand the mechanism of damage to these structures by cracking, a study based on the evaluation of the level

of damage by a calculation of the damage will be conducted in this paragraph. This is done to determine the criticality of the defects studied and consequently to identify the limits not to be crossed at the risk of causing failure.
The main characteristics of the polymers used in FDM/FFF have been classified in Fig. 1, with each characteristic ranked from lowest to highest. Each substance has unique characteristics, as shown in this graph. For example, PLA has been described as having superior layer adhesion during the FDM/FFF process and being a more easily printable material than other materials.

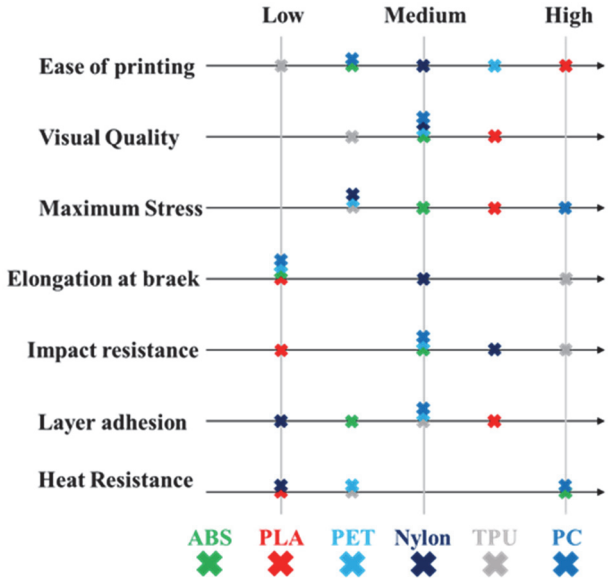

Figure 1: Representation of the characteristics of the materials applicable in the FDM/FFF process.

Analytical determination of Weibull elements

To evaluate the reliability of the results of the experimental tests conducted on 18 rectangular printed PLA specimens, each comprising 6 samples oriented at 0°, 45° and 90° fabricated using a FLASHFORGE 3 PRO 3D Printer with an extruder temperature of 215°C, a bed temperature of 80°C, a print speed of 60 mm/s, a layer height of 0.2 mm, and an infill density of 100%, we performed a statistical study using the Weibull distribution. This approach allows us to characterize the different zones of behavior, namely elasticity, stable plasticity, and unstable plasticity. Studying a statistical technique that allows us to estimate the elastic and maximum stresses that can be applied.
A specimen follows the Weibull statistic if there are two parameters: Weibull modulus (m) and a constant σ_0 such as we have:

$$\ln\ln\left(\frac{1}{P_s}\right) = m\left(\ln\sigma - \ln\sigma_0\right) \tag{1}$$

The next step is to plot. $\ln\ln\left(\frac{1}{P_s}\right)$ as a function of $\ln\sigma$. If the data points form a straight line, then the Weibull distribution can be used to model the data.

Calculation of static damage using the residual stress method

To assess the degree of degradation of the structures studied, it is necessary to measure the level of damage. The latter is directly related to physical properties, hence the importance of adopting a model of damage as a function of the stress state of the structure studied, which is related to the β life fraction, and consequently, the choice of the model of static damage, the expression of which is as follows:

$$Ds = \frac{1-\frac{\sigma_{ur}}{\sigma_u}}{1-\frac{\sigma_a}{\sigma_u}} \tag{2}$$

The β life fraction is defined as follows:

$$\beta = \frac{\boldsymbol{a}}{\boldsymbol{w}} \tag{3}$$

with :

$\boldsymbol{a}$: crack length for the case of a single notch

$\boldsymbol{w}$: the width of the notch;

$\boldsymbol{\sigma_{ur}}$: the residual ultimate stress;

$\boldsymbol{\sigma_u}$: the ultimate stress of the virgin material;

$\boldsymbol{\sigma_a}$: the stress just before the break.

In order to be able to draw the static damage curve, it is first necessary to determine the stress just before failure for the different structures studied.

$$f(\beta) = \frac{\boldsymbol{\sigma_{ur}}}{\boldsymbol{\sigma_u}} \quad \text{For} \quad \beta = 1 \;\; ; \;\; \frac{\boldsymbol{\sigma_{ur}}}{\boldsymbol{\sigma_u}} = \frac{\boldsymbol{\sigma_a}}{\boldsymbol{\sigma_u}} \tag{4}$$

and consequently, the evaluation of reliability becomes indispensable in any study of the mechanical behavior of components. In this section, we will present a reliability study to reduce the probability of sudden failure. The expression of static reliability is given by:

$$Rs(\beta) + F(\beta) = 1 \tag{5}$$

Calculation of damage by the unified theory method

In the literature, there are various models of damage coupled with measured residual resistance; Among these theories is the law of the "unified theory" which links damage to the variation of the endurance limit in a power function whose form:

$$D = \frac{\beta}{\beta + (1-\beta)\dfrac{\gamma - \left(\dfrac{\gamma}{\gamma_u}\right)^m}{\gamma - 1}} \tag{6}$$

$$\gamma_d = \left(\frac{\gamma}{\gamma_u}\right)^m \tag{7}$$

$$\gamma_u = \frac{\sigma_u}{\sigma_0} \tag{8}$$

$$\gamma = \frac{\sigma_{ur}}{\sigma_0} \tag{9}$$

σ_0: The residual endurance limit of the virgin material, which is equal to the ultimate residual stress multiplied by a coefficient α:

$$\alpha = \frac{1}{\textbf{\textit{Material Safety Factor}}} \tag{10}$$

Specimen preparation

The 3D printed SENT specimen, while not conforming to ASTM standards, has been the subject of extensive research by ASTM regarding fracture strength evaluation. Originally proposed in 1962 by Irwin, Krafft, and Sullivan, the SENT specimen concept is utilized to assess the elastic plane strain fracture toughness (K_{Ic} or G_{Ic}). Throughout the years, scholars such as Sullivan, Srawley, and Tada have made significant contributions to elucidating the behavior of SENT specimens. Nevertheless, ASTM's primary emphasis has transitioned towards measuring the minimum resistance to plane deformation, resulting in the prevalence of high-stress bending specimens like CT and SENB in conventional fracture toughness testing methodologies. The inaugural ASTM E399-72 standard for fracture toughness testing of K_{Ic} was issued in 1972.

The 3D-printed PLA Single Edge Notch Tension (SENT) specimens were fabricated using a FLASHFORGE 3 PRO 3D Printer with the previously mentioned parameters. The specimens, measuring 100 x 20 x 2 mm³, were then manually pre-cracked with a razor blade for SENT testing (see Fig. 2).

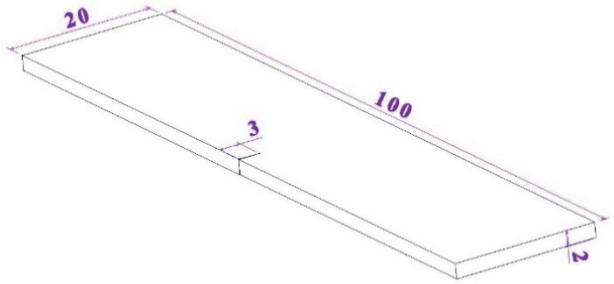

Figure 2: Dimensions of PLA printed specimens.

In the experimental procedure, the samples underwent a two-step coloring process. Initially, the entire surface of the samples was uniformly coated with white paint as shown in Fig. 3. This step served as a preparatory measure and avoid the paint drips, creating a neutral base that facilitated the subsequent application of a distinct and high-contrast pattern.

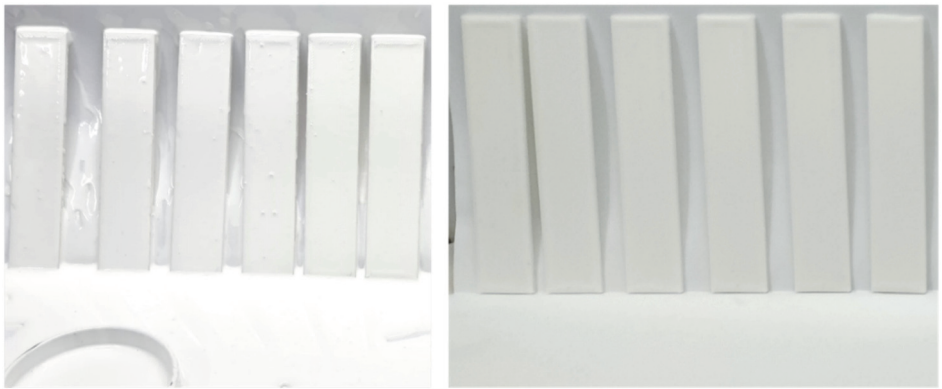

Figure 3: Uniform coating of white paint across the entire surface of the samples.

Following the white base coat, the targeted spraying process was initiated using black spray paint. The objective was to create a well-defined pattern on the samples, crucial for accurate DIC measurements. As illustrated in Fig. 4, by carefully adjusting the spraying distance and focusing on the surrounding area of the test specimen, the process aimed to minimize the average size of the pattern while ensuring even coverage. It's important to note that this procedure is intended for the next study and not for the current one.

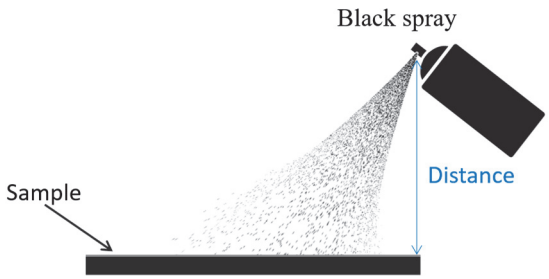

Figure 4: Diagram of the spray method for pattern making.

A good pattern must meet several requirements to perform accurate DIC measurements. To ensure patterns consistent with the literature, an attempt was made to optimize the spray distance to decrease the average pattern size and reduce dispersion, targeting the specimen area so that the larger particles fall within a few centimeters of the nozzle and thus do not reach the target (as shown in Fig. 4), using a can of black paint. Its result is shown in Fig. 5.

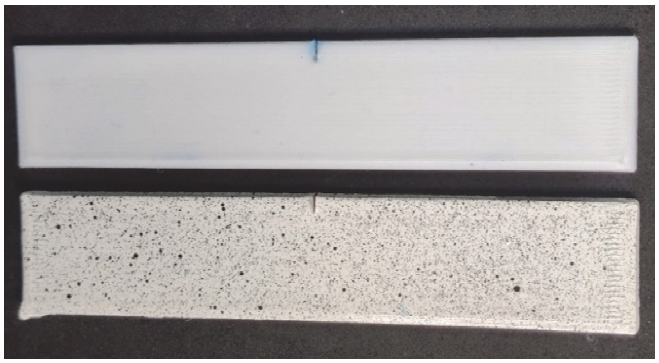

Figure 5: Effect of spray distance optimization on pattern consistency for Digital Image Correlation (DIC) measurements.

Experimental design

A uniaxial tensile test was performed using an MTS tensile testing machine. The experiments are piloted on the move with a traverse speed of 1mm/min. The tensile test was recorded using an IDS UI-3880CP camera. The experimental field was illuminated by an essential light bar of 15 blue LEDs +/- 25° with a polarizer to ensure the image capture conditions during the tests (Fig. 6).

The excellent choices for FDM/FFF printing are graphically illustrated in Fig. 4, where ABS, PLA, and nylon are highlighted for their well-balanced blend of mechanical qualities, printability, and aesthetic appeal. ABS and PLA materials stand out as the most user-friendly due to their tolerance in different printing parameters and their low risk of deformation or delamination. Even though nylon adds a little more complexity, it's still possible to do so throughout the FDM/FFF printing process. On the other hand, PC, which is considered the most difficult material to print with FDM/FFF, is preferred for uses involving high temperatures. ABS and PC materials have the highest maximum stress values, indicating their greater durability, while PLA and nylon lag a bit, but still show sufficient strength for a variety of FDM/FFF applications. PLA and nylon, on the other hand, exhibit remarkable strength while having a higher fracture deformation than ABS and PC, which also have the lowest fracture deformation, indicating less brittleness. ABS and PC are particularly resistant to impacts, which reduces the risk of falls or impacts. For ABS, PLA, and nylon, layer adhesion, a crucial component of FDM/FFF printing, is satisfactory, adding to their overall delamination resistance. Compared to other materials, PC has a somewhat weaker layer adhesion. The PC stands out for its strongest heat resistance, capable of tolerating temperatures of up to 250 degrees Celsius. For FDM/FFF applications that require exposure to high temperatures, this makes PC the best option. Although PLA and nylon have the lowest heat resistance and should not be exposed to temperatures above 60 degrees Celsius, ABS has a lower heat resistance of up to 100 degrees Celsius, making it suitable for FDM/FFF environments with moderate temperatures. To summarize, Fig. 5 summarizes the extensive research and highlights ABS, PLA, and nylon as good choices for FDM/FFF printing. It also suggests a PC for applications that require resistance to high temperatures.

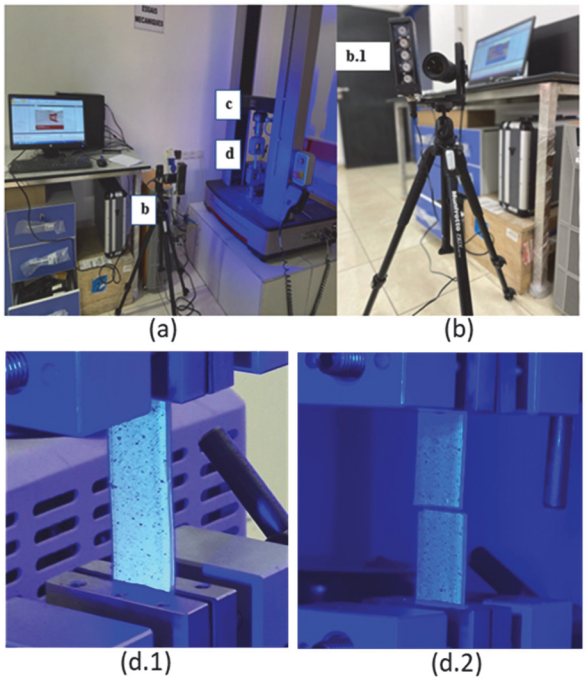

Figure 6: (a) Tensile test system; (b) DIC System; (b.1) LED light source; (c) MTS Testing Machine; (d.1) specimen before deformation; (d.2) Specimen after rupture.

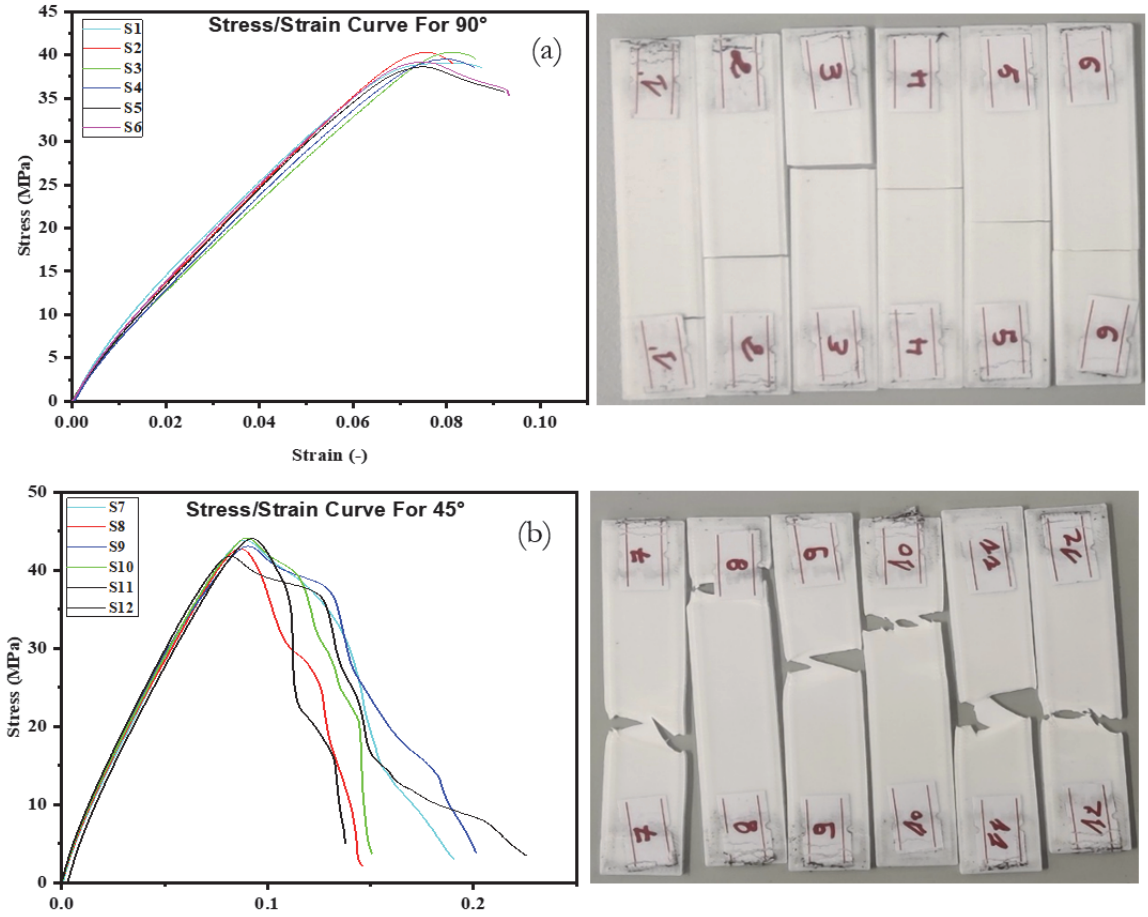

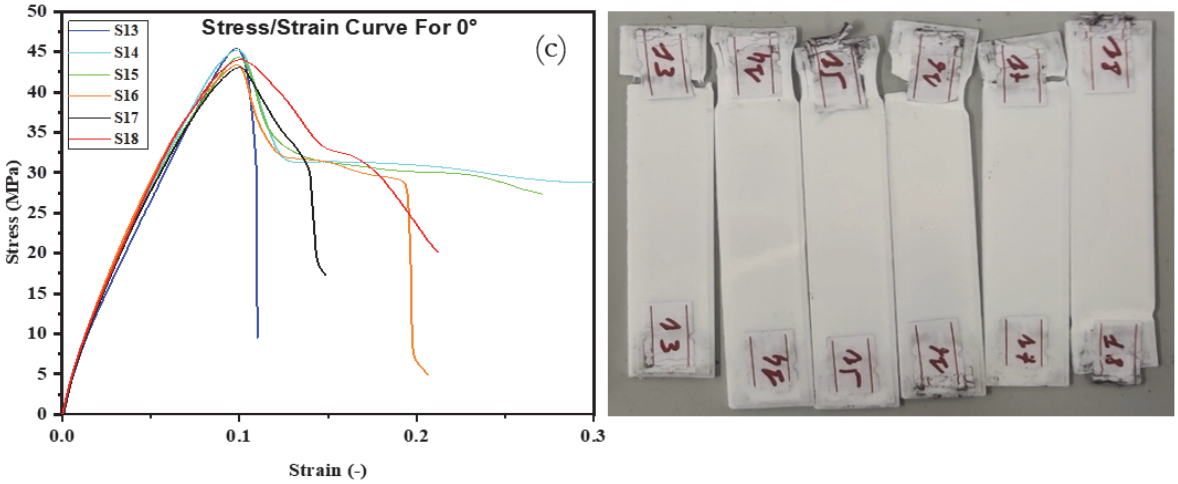

Figure 7: Impact of filament orientation on tensile strength and strain in 3D Printed PLA Samples.

RESULT AND DISCUSSION

Statistical analysis of 3D printed samples

The curves presented in Fig. 7 show distinct stress and strain behaviors. The 0° orientation curves (colored and non-colored) reach the highest stress levels before dropping sharply, indicating the greatest tensile strength. This aligns with the fact that infill lines aligned with the loading direction contribute to better mechanical performance. Conversely, the 90° orientation curves (colored and non-colored) show the lowest stress levels throughout the strain, indicating the lowest tensile strength. This is because the infill lines are perpendicular to the loading direction, offering minimal resistance to the pulling force. 45° and 90° orientations: In contrast, when the infill lines are at 45° or 90° orientations, they are not directly aligned with the pulling force. It is like trying to support the same object by placing it at an angle on the pillars. The angled orientation makes it easier for the object to slide off or for the pillars to break, leading to lower overall strength.

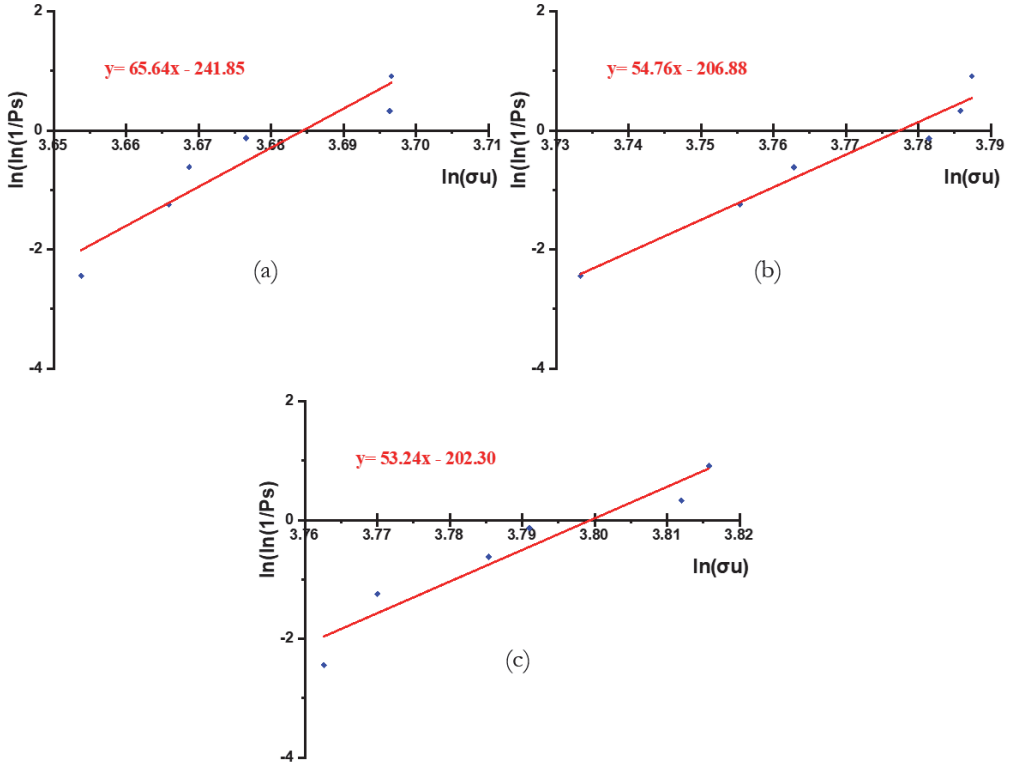

Figure 8: Weibull distribution analysis of tensile strength at different orientations (a): 90°, (b): 45°, and (c): 0°.

For maximum stress

These results plotted in Fig. 8 present the Weibull distribution at three different angles (90°, 45°, and 0°), analyzing the tested samples' ultimate stress and fatigue life characteristics. Three linear regression lines are plotted to model the relationship between these variables, with the respective equations: y = 65.6x - 241.85 for the 90° angle, y = 54.76x - 206.88 for the 45° angle, and y = 53.24x - 202.30 for the 0° angle.

All of these equations are summarized in Tab. 2. These graphs and equations allow for the analysis of variations in ultimate stress and fatigue life as a function of sample orientation, providing crucial information for understanding the mechanical behavior of the materials under test.

The values of σ_{u0} obtained experimentally for each orientation are almost identical to those calculated analytically.

Samples	Equation	m	σ_{u0} (MPa)
90°	y= 65.64x - 241.85	65.64	39.82
45°	y= 54.76x - 206.88	54.76	43.72
0°	y= 53.24x - 202.30	53.24	44.69

Table 2: Weibull regression equations for different orientations with baseline scale parameter σ_{u0} (MPa).

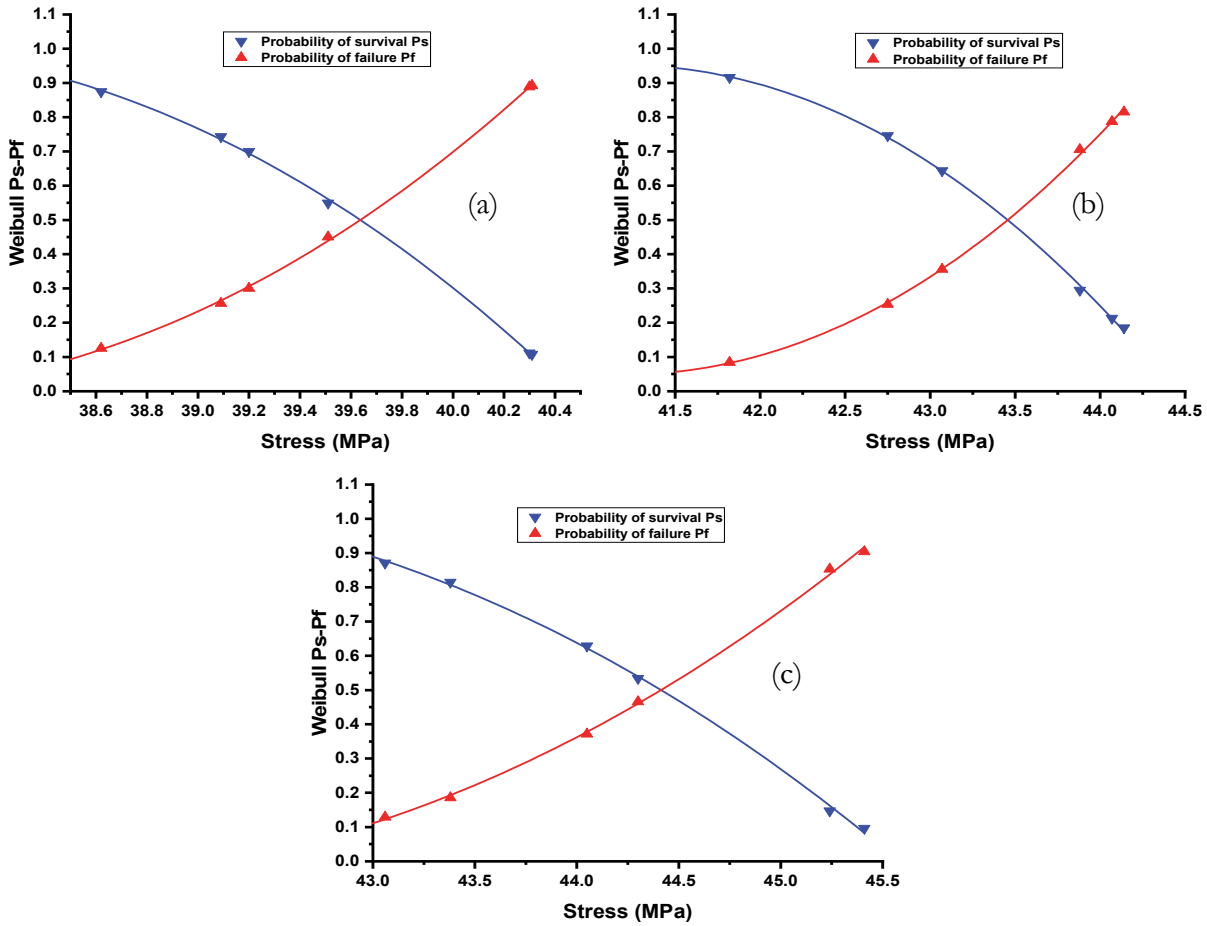

Figure 9: Probability of Survival (Ps) and Probability of Failure (Pf) for different specimen orientations: (a) 90°, (b) 45° and (c) 0°, as a function of stress (MPa).

The three graphs (a), (b), and (c) in Fig. 9 represent the probability of survival (Ps) and probability of failure (Pf), respectively, for specimens oriented at 90°, 45°, and 0°.

Each graph has two distinct curves: the blue curve represents the probability of survival Ps, while the red curve represents the probability of failure Pf as a function of ultimate stress (MPa).

In Fig. 9(a), which corresponds to the specimens oriented at 90°, the probability of survival decreases, and the probability of failure increases as the stress increases. In Fig. 9(b), which shows the specimens oriented at 45°, there is also a decrease in the probability of survival and an increase in the probability of failure with increasing stress. Finally, in Fig. 9(c), which relates to specimens oriented at 0°, the trends in the probability of survival and failure are similar to the other two cases, with a decrease in the probability of survival and an increase in the probability of failure with increasing stress.

For elastic stress

The results presented in Fig. 10 provide valuable information about the mechanical properties of 3D printed samples in different orientations. In the 90° orientation Fig. 10(a), the positive slope of the linear regression line y=77.68x−277.26 indicates that the electrical stress (σe) increases with fatigue life (Nf/PS). This suggests that samples oriented at 90° have a less ability to withstand cyclic loads. This improvement can be attributed to a more efficient distribution of stresses along the filaments when the applied forces are aligned with the predominant direction of the filaments. In the 45° orientation Fig. 10(b), the less steep slope of the y=42.5x−154.26 regression line suggests a similar relationship between elastic stress and fatigue life, although less pronounced than in the 90° orientation. This sample orientation configuration can result in a relatively uniform distribution of forces on the filaments, resulting in slightly lower resistance to repeated stresses compared to the 90° orientation. In the 0° orientation Fig. 10(c), the positive slope of the y=39x−142.99 regression line also indicates a relationship between ultimate stress and fatigue life, although better than in the other orientations. Physically, in this orientation, the forces applied are parallel to the direction of the filaments, which can result in different mechanical properties. This results in better resistance to cyclic loads compared to other orientations.

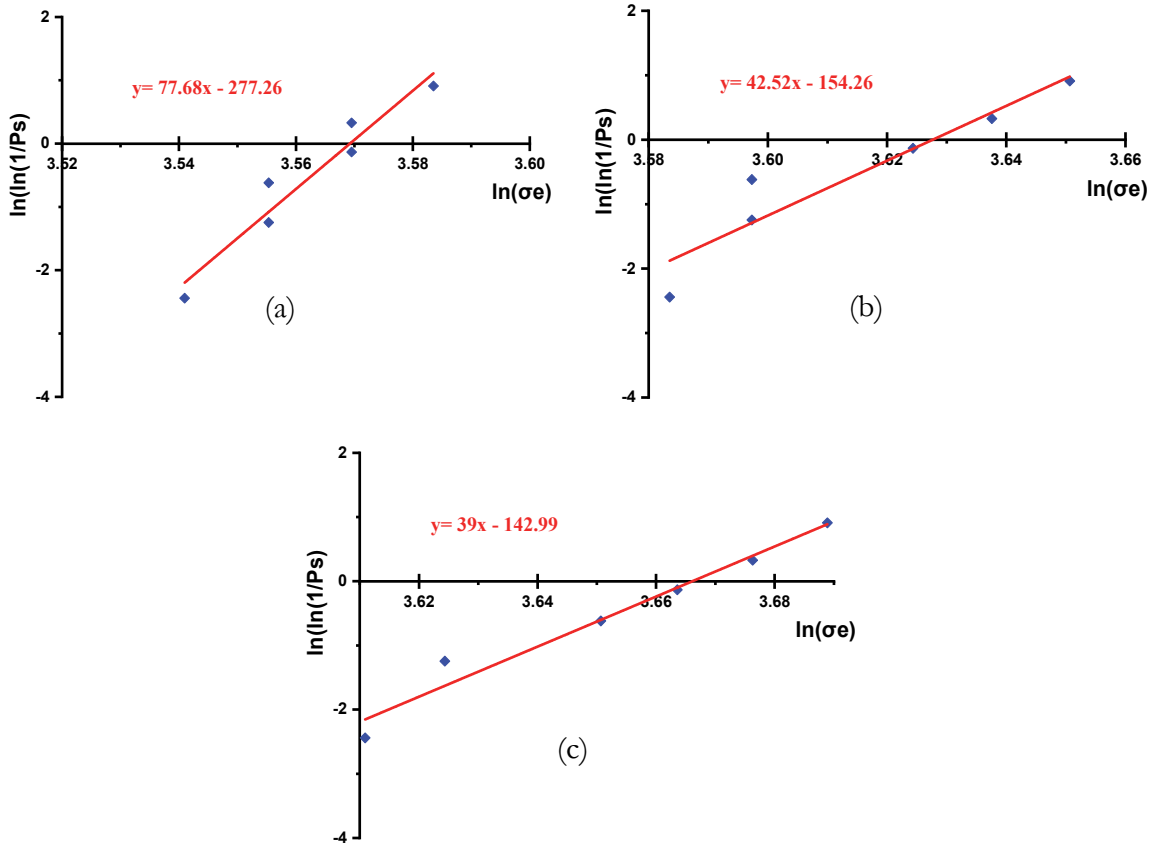

Figure 10: Weibull distribution analysis of elastic strength at different orientations (a): 90°, (b): 45°, and (c): 0°.

Tab. 3 summarizes the regression equations for each orientation, providing a baseline for the observed relationships between electrical stress and fatigue life in each sample orientation configuration. The values of σe0 obtained experimentally for each orientation are almost identical to those calculated analytically.

Samples	Equation	m	σ_{e0} (MPa)
90°	y= 77.68x - 277.26	77.68	35.49 MPa
45°	y= 42.52x - 154.26	42.52	37.63 MPa
0°	y= 39x - 142.99	39	39.11 MPa

Table 3: Weibull regression equations for different orientations with baseline scale parameter σ_{e0} (MPa).

In each graph in Fig. 11, the probability of survival (Ps) curves in blue and the probability of failure (Pf) curves in red intersect, illustrating crucial relationships between stress and associated probabilities. In Fig. 11(a), a linear relationship emerges: as the stress increases, the Ps decreases while the Pf increases. This observation is significant for materials or systems where increased stress makes failure more likely. In Fig. 11(b), although the relationship is similar to that in Fig. 11(a), the values differ. The probability of survival decreases and the probability of failure increases with increasing stress, highlighting a general trend in different contexts. Fig. 11(c) shows a more pronounced curvature at the point of intersection of the Ps and Pf curves, indicating a sharper transition between the probabilities of survival and failure around certain stress values.

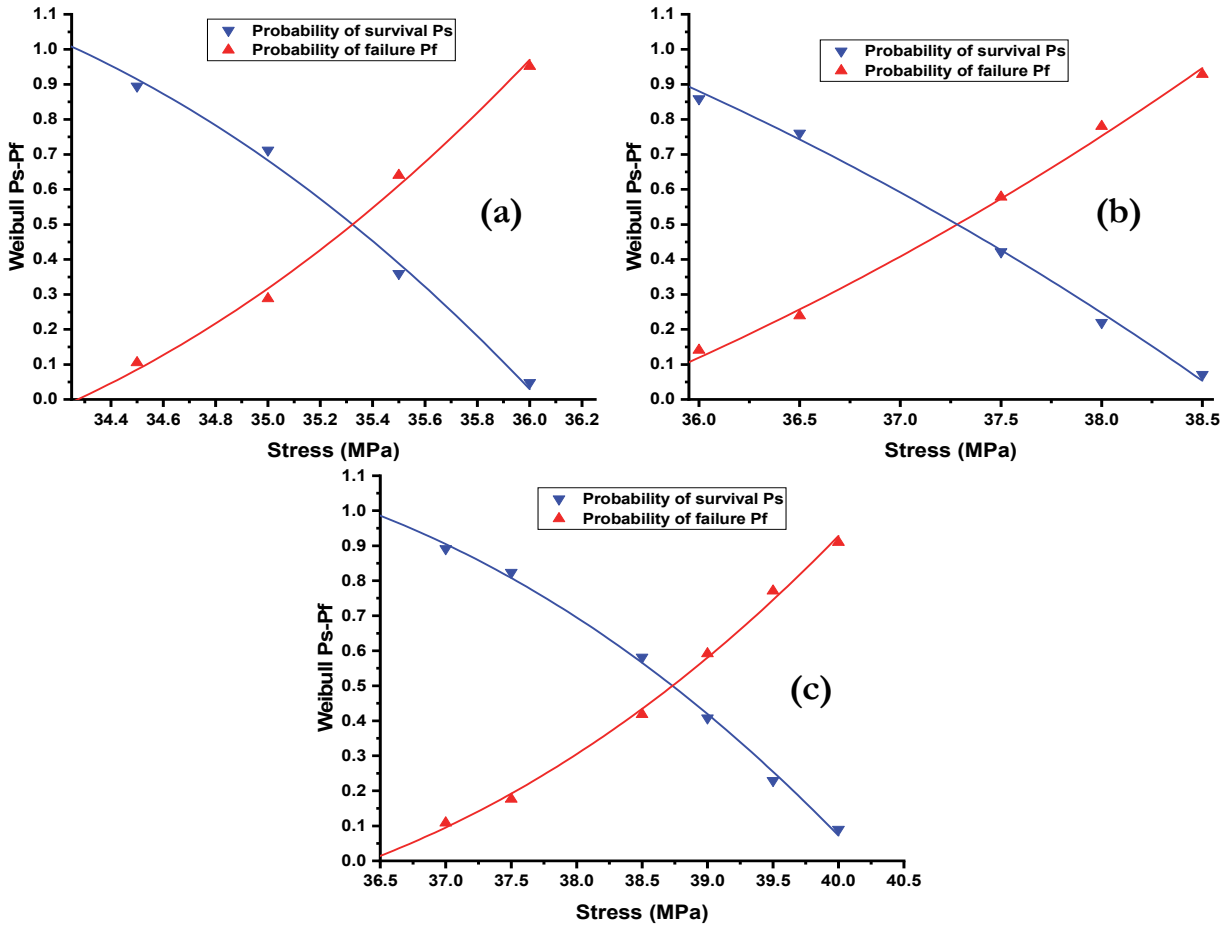

Figure 11: Probability of Survival (Ps) and Probability of Failure (Pf) for different specimen orientations: (a) 90°, (b) 45° and (c) 0°, as a function of stress (MPa).

The results in Fig. 12 suggest that the behavior of the material depends on its orientation relative to the direction of the applied force. In general, materials exhibit mechanical anisotropy, i.e., their properties (including strength) vary with direction. In the 90° orientation (Fig. 12(a)), the stress ranges are from 0 MPa to 35 MPa for Zone I, from 35 MPa to 40 MPa for Zone II, and are greater than 40 MPa for Zone III. Similarly, in the 45° orientation (Fig. 12(b)) and in the 0° orientation (Fig. 12(c)), the stress ranges show consistent variations. In the 45° orientation, Zone I range from 0 MPa to 37

MPa, Zone II from 37 MPa to 42 MPa, and Zone III is greater than or equal to 42 MPa. As for the 0° orientation, Zone I range from 0 MPa to 38.5 MPa, Zone II from 38.5 MPa to 44 MPa, and Zone III is greater than or equal to 44 MPa. This may be due to anisotropic properties of the material, such as a crystal structure or a predominant molecular orientation. This directional variation in strength can be significant in applications where loads are applied in specific directions, requiring careful consideration when designing and using materials.

Zone I is the range where the material behaves elastically. This means that the material reversibly deforms when stress is applied, and it returns to its original shape once the stress is released. This area indicates some flexibility of the material within this stress range. Zone II represents the region of stable plastic deformation. Beyond a certain stress value, the material begins to undergo permanent deformation, but this deformation remains stable and reversible within this stress range. This means that the material can retain its ability to support the load without suffering catastrophic failure; Zone III corresponds to the strength limit of the material. Beyond a certain stress value, the material reaches its strength limit and can suffer irreversible failure. Deformation in this area becomes unstable and can lead to abrupt breakage of the material.

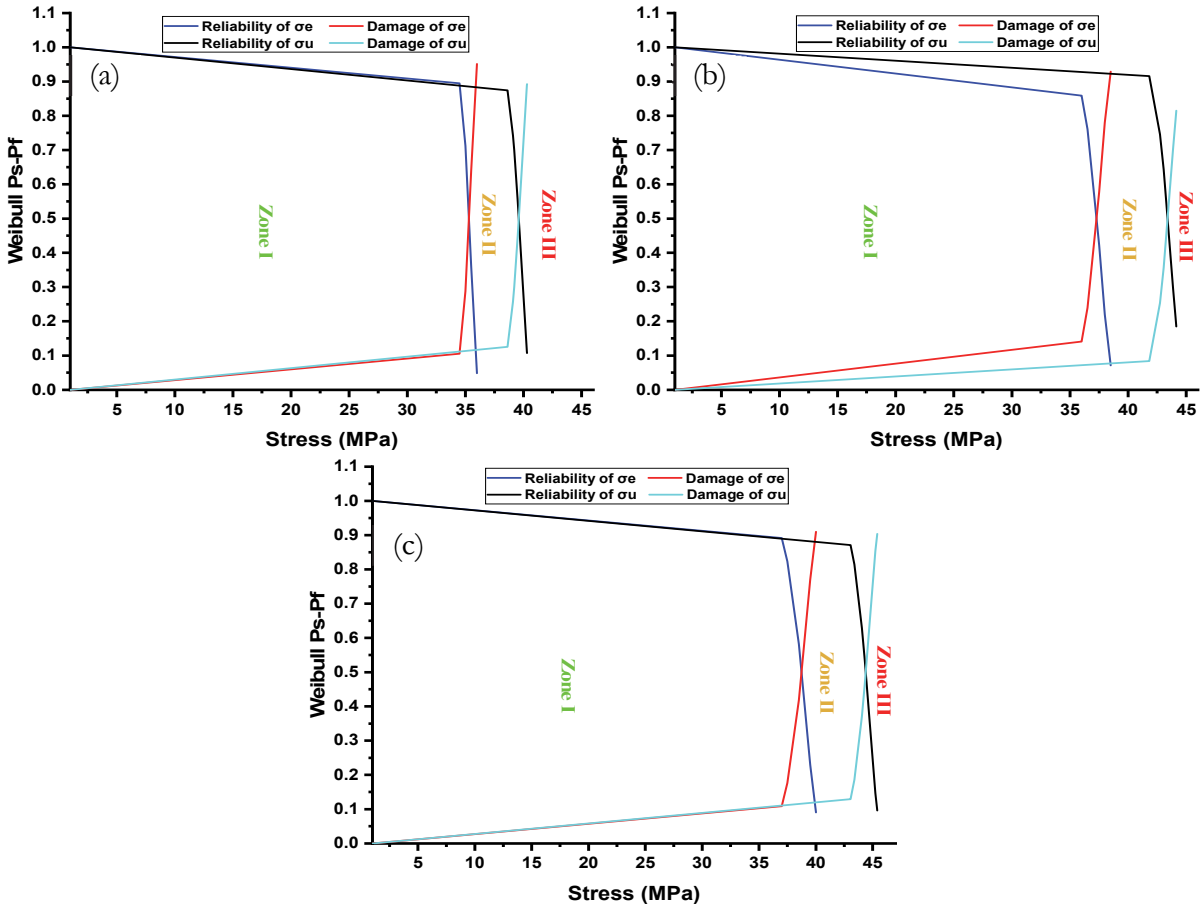

Figure 12: Reliability and damage of the Weibull depending on σ of ABS specimens.

Effect of white print on the mechanical properties

A tensile test was conducted on six printed SENT (Single-Edge Notched Tension) samples. These samples were divided into two groups: three and three, not colored. Each group was tested at three different orientations: 0°, 45°, and 90°. These samples were divided into two groups: three colored and three not colored. Each group was tested at three different orientations: 0°, 45°, and 90°. Your primary focus is to interpret the effect of printing used, specifically the color, on the mechanical behavior of these samples.

As a result of Fig. 13 stress-strain curves for the colored and non-colored samples at each orientation (0°, 45°, and 90°) nearly overlay each other, which suggests a minimal influence of color on the mechanical properties.

The result indicates that adding a white color fine surface through colored printing did not have a discernible impact on the mechanical properties of the tested samples. The comparison between three samples without any surface treatment (referred to as "not colored") and three samples with a white color fine surface (referred to as "colored printing") revealed no

significant differences in terms of tensile strength, yield strength, or elongation. This suggests that the colored printing process employed in this study does not adversely affect the material's response to tensile loading. The mechanical integrity of the material remained consistent, regardless of the surface treatment. This result is valuable as it implies that adding a fine white color surface, at least through the method employed in this study, does not compromise the material's performance under tensile stress conditions.

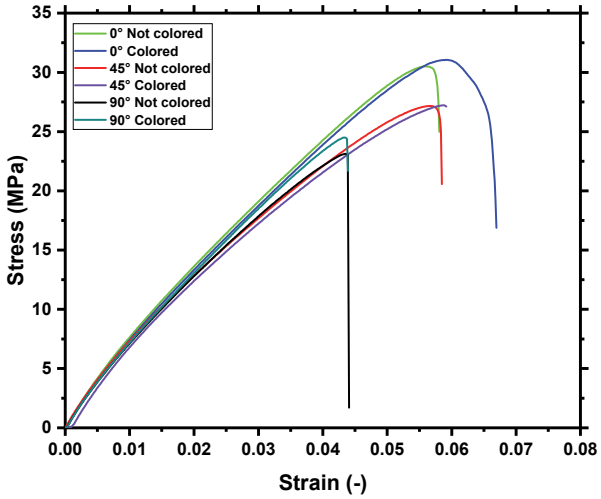

Figure 13: Stress-Strain behavior of colored and non-colored samples orientations.

Effect of increasing crack length on the tensile mechanical behavior of PLA

Following the tensile curves in Fig. 14, specimens with initial notches (E1-E5, E7-E11, and E13-E17) have a lower tensile strength than specimens without a notch (blank) (E6, E12, and E18), and this strength gradually decreases as the notch size increases.

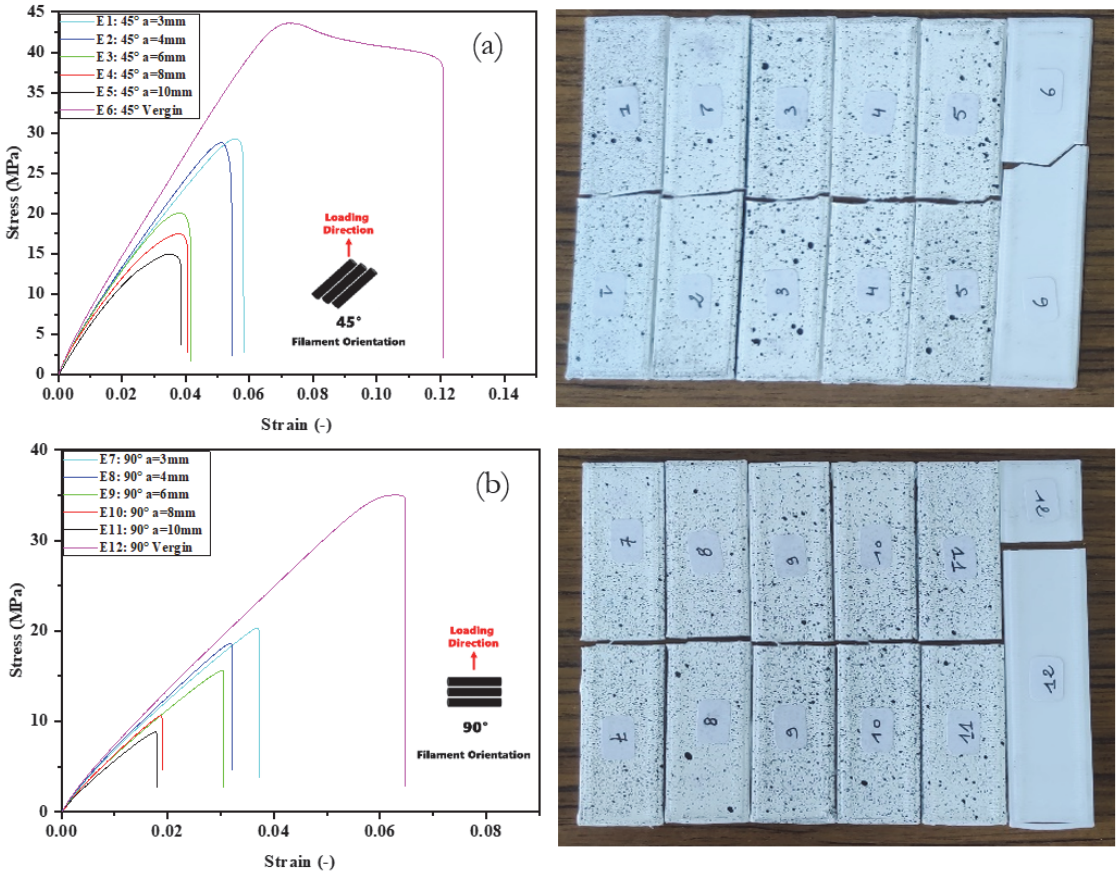

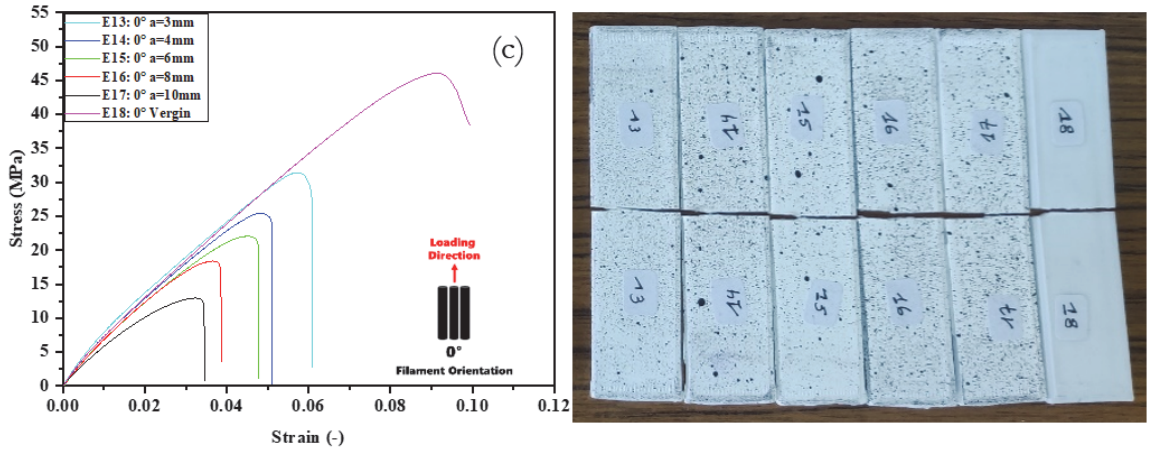

Figure 14: Effect of the increase of the crack length on the Stress-Strain Behavior (a): 45°, (b): 90°, and (c): 0°

At the same time, the stress-strain curves of the notched specimens show a shorter plastic strain zone than that of the non-notched specimen, indicating lower ductility of the material and easier breakage. These observations shed light on the effects of notches on the mechanical behavior of the material: they create stress concentration points, weakening the material and reducing its tensile strength. In addition, the magnitude of this attenuation is directly proportional to the size of the notch. This is due to the creation of stress concentration points in the notch area, where the stress is higher than in the undamaged areas. These stress concentration points can initiate material failure, leading to premature failure. Notches, even small ones, can have a significant impact on the tensile strength and ductility of the material.

These results highlight the importance of minimizing defects in materials to ensure optimal mechanical performance. Notches, even small ones, can have a significant impact on the tensile strength and ductility of the material. The figure also shows that the relationship between notch size and tensile strength is progressive. This means that there is no threshold below which the nick has no effect. Any notch, no matter how small, will weaken the material to some extent.

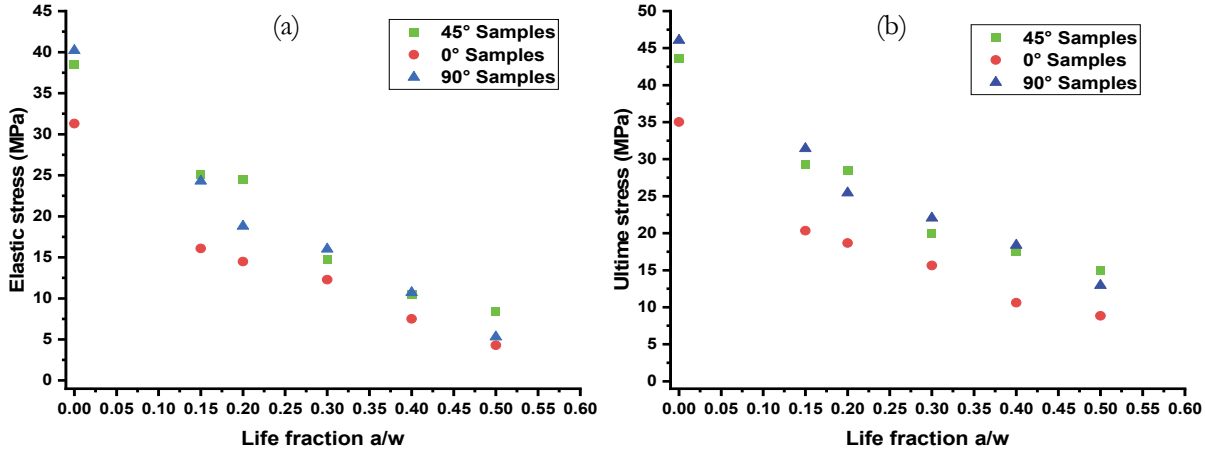

Figure 15: Deterioration of residual stress as a function of life fraction (a): Elastic stress, (b) Ultimate stress.

Fig. 15 shows that, there is a remarkable deterioration of the residual ultimate stress with the evolution of the size of the defect, represented here by the life fraction $\beta = \frac{Crack\ lenth}{sample\ width}$ of the types of defects studied. It can be deduced that the behavior of the material is impacted by the presence of defects, which results in the degradation of these mechanical properties and, consequently, the material tends to become more brittle, which leads to an increasingly abrupt breakage. The curves representing the dimensionless stress as a function of the fraction of life are given in Fig. 16.

After determining the stress just before breaking for all the specimens studied, the figures below illustrate the behavior of the damage between the undamaged specimen in its virgin state, which corresponds to zero damage, and the damaged specimen, which has a damage value of 1, for each type of defect.

Fig. 17 illustrates the standardized experimental damage progression and reliability for the fraction of life (β), with each case implying a different focus to be examined. The damage process is illustrated by a concave curve, indicating an acceleration of the damage towards the end of the material's life at D = 1. Increased damage leads to increased elongation and reduced modulus of stress and elasticity in static tensile testing of PLA samples. This means damage characterized by noticeable irreversible deformations, which eventually decrease the ultimate strength of the material.

The Material Safety Factor (MSF) for PLA (Polylactic Acid) filament can vary depending on its application and the specific requirements of a project. However, the typical value for the Material Safety Factor for PLA used in 3D printing is around 1.5 to 2.0.

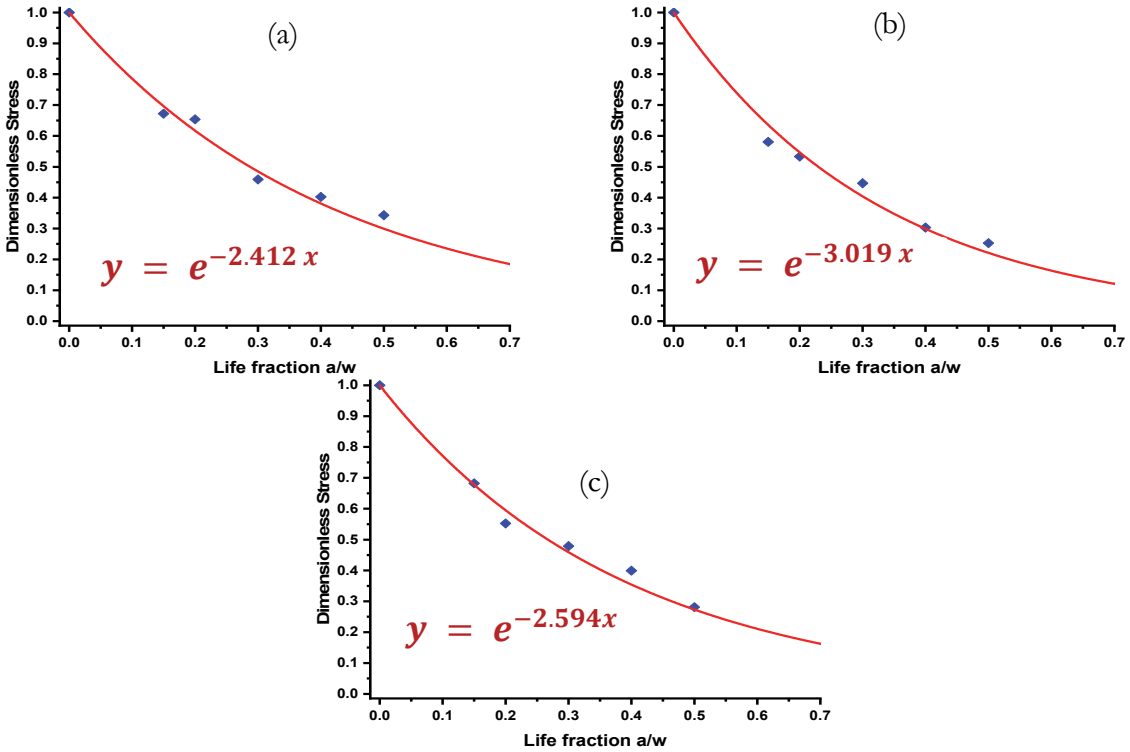

Figure 16: Dimensionless stress as a function of the fraction of life (a): 45°, (b): 90°, and (c): 0°.

The damage is subject to an increase in transient crack length between zero (virgin) and their critical crack length. The configuration and extent of the end-of-life damage of the material (D = 1, β = 1) lends some credibility to this experimental model of damage, consistent with the results of a related polymer study. The establishment of normalized damage is an essential experimental reference point for validating theoretical models or alternative methods of assessing experimental damage. The ability to correlate the damage process with the three stages of damage is particularly intriguing. The examination of the damage curves represented by the ultimate stress, initially, at the beginning of the damage, i.e. at the culmination of stage I, corresponds to the initial phase of the material's life, It starts at the leftmost part of the graph (near x=0) and extends to the first dashed line (green). where the life fraction β (a) = 27%, β (b) = 19%, and β (c) = 25.5%, the damage increases concave and progressively. Subsequently, during the progressive phase, called stage II. At this point, the accumulated damage increases faster. The material undergoes moderate wear and degradation the damage increases regularly, where the life fraction is β (a) [27%, 58%], β (b) [19%, 52%], β (c) [15.5%, 63%]. Then, reaching the stage of abrupt propagation, where the fraction of beta life is greater than 50%, resulting in D = 0.75. The cumulative damage increases significantly, approaching the maximum value (y=1). The material is likely close to failure or has reached its end-of-life condition where a significant acceleration of damage culminates in a material failure.

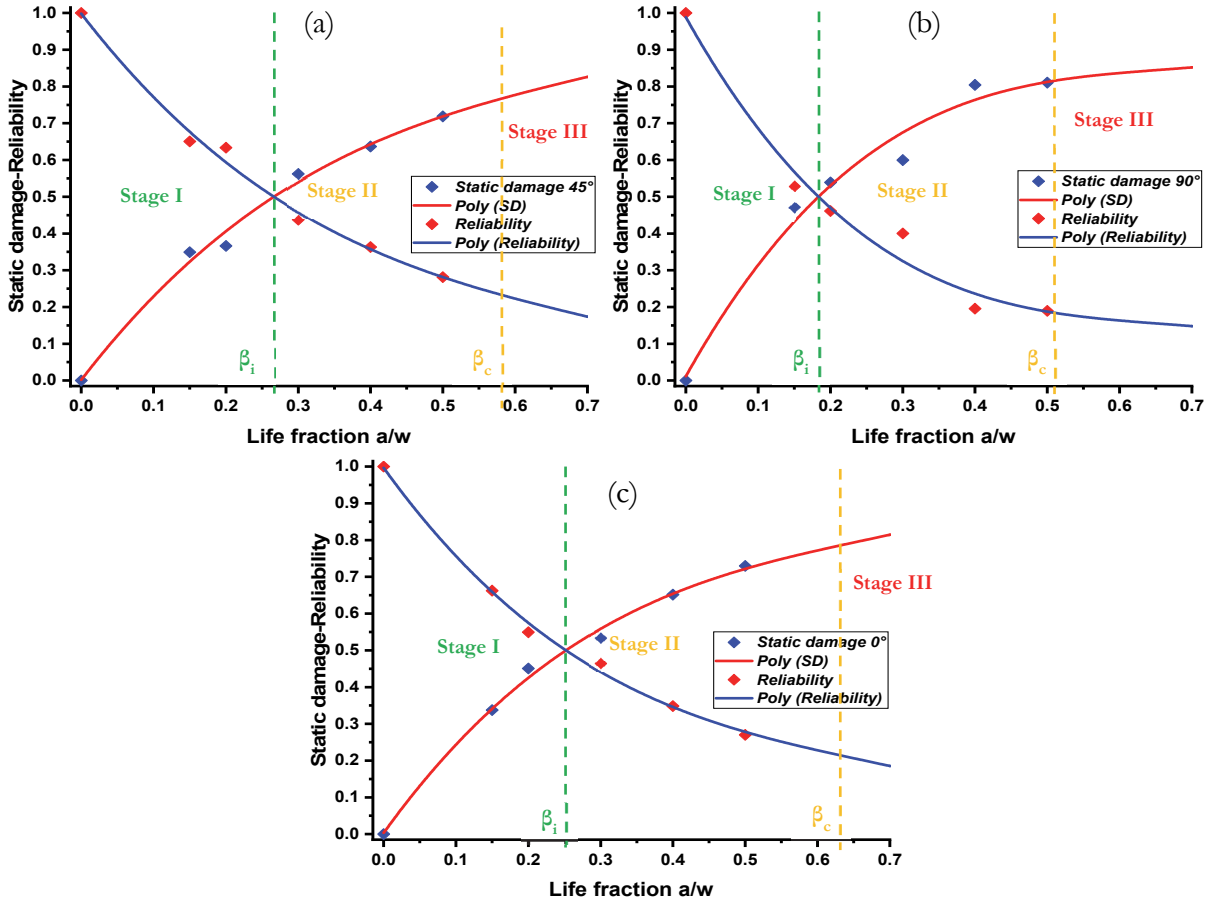

Figure 17: Evolution of experimental static damage and reliability as a function of life fraction (a): 45°, (b): 90°, and (c): 0°.

Relationship static damage and static reliability.

According to the results of the previous section, it can be seen that the curves representing static damage-reliability have the same appearance for the different orientations studied, although the characteristics sampled differ in value according to the type of orientation. Therefore, a comparative study was established to identify the criticality of each orientation. Fig. 18 below shows all the Damage-Reliability curves of the different specimens.

It is clear from Fig. 18 above that the reliability curves evolve in the opposite direction to that of the damage with the same rate, which is reflected in the relationship.

Fig. 18 illustrates the evolution of static damage-reliability as a function of life fraction for different orientations. Regardless of the orientation used, the damage rate gradually increases from 0 to the critical value of 1. The increase in cracking leads to a more pronounced decline in the mechanical characteristics of the PLA. This underlines the ability of this particular mechanical tensile characteristic to effectively follow the degradation trend resulting from crack evolution. The calculations derived from the ultimate stress modulus for each orientation show similarities, converging with 50% reliability, with a slight deviation of about 2% in terms of life fraction. The model proposed in this study provides valuable information on the state of the ultimate stress, even if it tends to overestimate material losses. In particular, it can be observed that the damage curve of the cracked specimen oriented at 90° is lower than that of the specimens oriented at 45° and 0° during the first two steps. This reflects the rapidly changing damage level of specimens oriented 90° the single notch compared to the others. Almost all curves merge from the critical life fraction βc, indicating the beginning of the third stage, which is an unstable phase where the damage becomes uncontrollable and the specimens can manifest a sudden failure at any time.

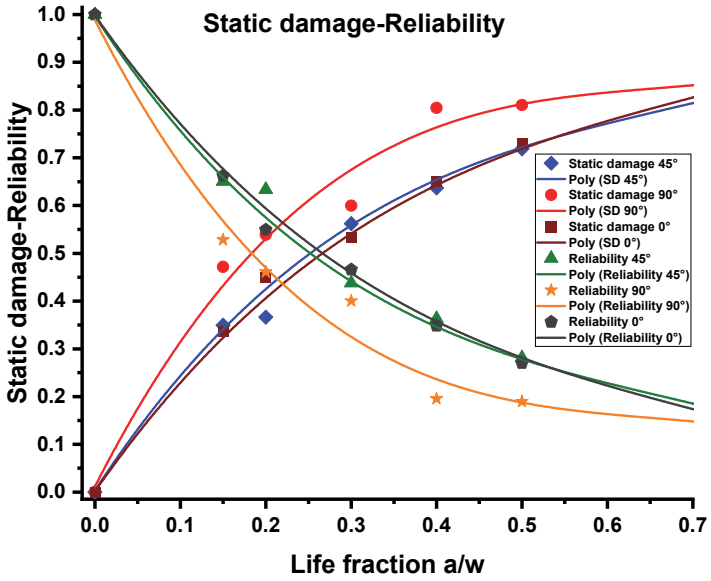

Figure 18: Evolution static damage and Reliability as a function of life fraction.

The different curves of the damage by unified theory as a function of the life fraction β are given in Fig. 19. For polymers, m was taken equal to 1.

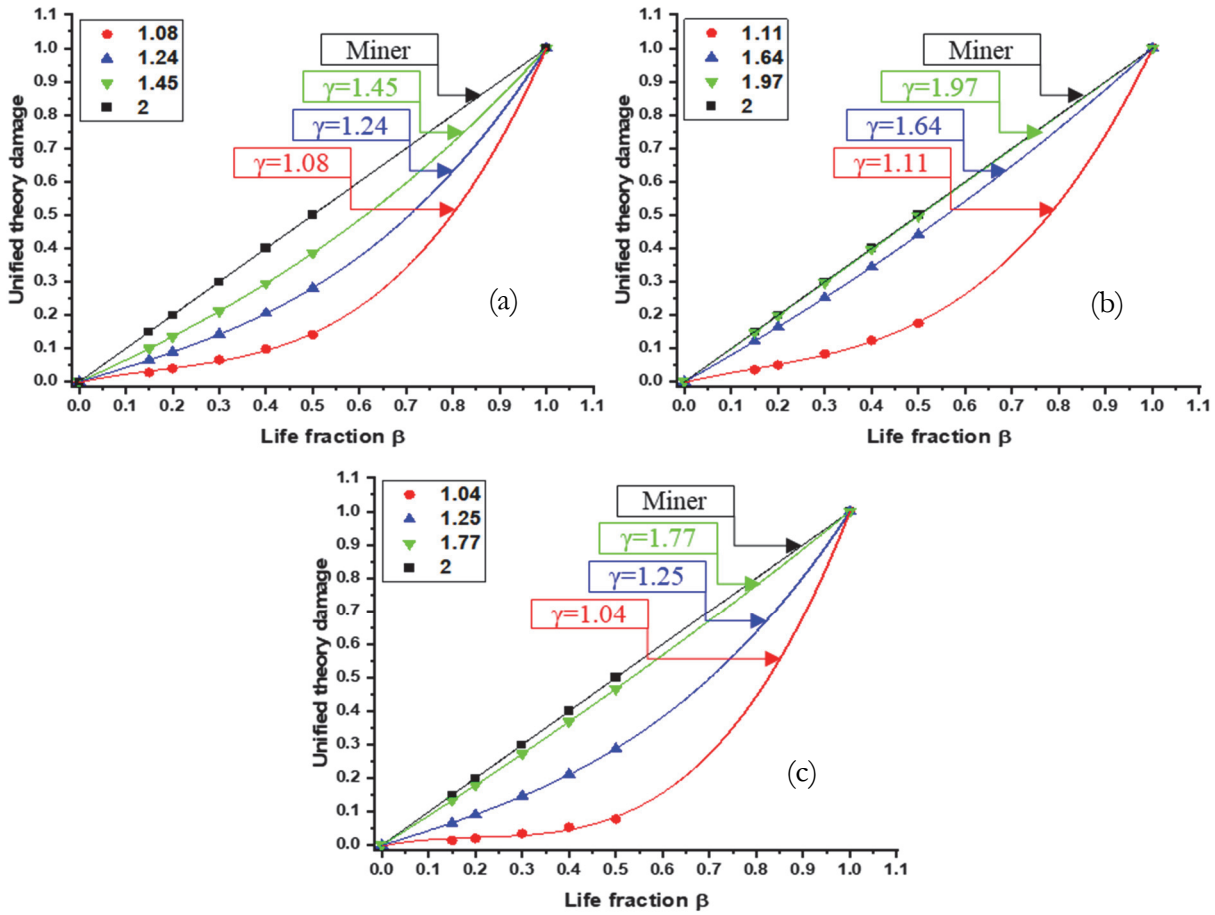

Figure 19: Curves of the unified theory Damage as a function of life fraction (a): 45°, (b): 90°, and (c): 0°.

Based on the analysis of the various figures representing damage according to the unified theory for each studied structure, it is evident that as the loading increases, the damage curve approaches the bisector corresponding to Miner's damage. This observation leads to the conclusion that Miner's rule provides a higher level of safety as the damage calculated by the unified theory remains underestimated compared to the static damage. Therefore, it is inferred that Miner's rule is commonly used in studies addressing structural damage due to its conservative nature and ability to provide a more secure design approach.

CONCLUSION

This study investigates the mechanical behavior of PLA specimens fabricated via Fused Deposition Modeling (FDM), focusing on mechanical characterization, damage evolution, and reliability across different print orientations.

- Tensile tests on specimens oriented at 0°, 45°, and 90° relative to the printing direction revealed Young's modulus of 0.9–1.2 GPa, the ultimate tensile stress of 39–44 MPa, and conventional yield strength of 35–38 MPa, highlighting orientation-dependent mechanical performance.
- Analysis of specimens with artificial cracks demonstrated that PLA's mechanical properties degrade with increasing defect size, with static damage scaling proportionally to the life fraction. A reliability study identified the critical crack length, pinpointing the most vulnerable specimen configuration.
- Larger cracks accelerated the decline in PLA's mechanical properties. Ultimate stress calculations showed consistent behavior across orientations, converging at 50% reliability with a minor ~2% variation in life fraction.
- Damage progression in 90°-oriented cracked specimens was more pronounced in the initial stages compared to 0° and 45° orientations, reflecting faster damage evolution. However, all damage curves converged at the critical life fraction (βc), marking the onset of an unstable phase where damage becomes uncontrollable, potentially leading to sudden failure.

To address crack propagation effectively, we propose a targeted solution: when a crack reaches 45% of its life fraction (βc = 0.5), the pre-cracked region is excised by reducing the specimen's width. This intervention eliminates the crack, prevents stress concentration at the crack tip, halts crack propagation, and significantly enhances the material's durability and structural integrity under challenging conditions.

REFERENCES

[1] Colorado, H.A., Cardenas, C.A., Gutierrez-Velazquez, E.I., Escobedo, J.P., Monteiro, S.N. (2023). Additive manufacturing in armor and military applications: research, materials, processing technologies, perspectives, and challenges, Journal of Materials Research and Technology, 27, pp. 3900–3913. DOI: 10.1016/J.JMRT.2023.11.030.

[2] Cózar, I.R., Otero, F., Maimí, P., González, E. V., Miot, S., Turon, A., Camanho, P.P. (2022). A three-dimensional plastic-damage model for polymer composite materials, Compos Part A Appl Sci Manuf, 163, p. 107198.

[3] Fehreddine, M.R., Gábor, B., Zsolt, L. (2022). Optimization of notched tensile test specimen under plane strain condition, Multidiszciplináris Tudományok, 12(3), pp. 117–126.

[4] Guessasma, S., Belhabib, S., Nouri, H., Ben Hassana, O. (2016). Anisotropic damage inferred to 3D printed polymers using fused deposition modelling and subject to severe compression, Eur Polym J, 85, pp. 324–340. DOI: 10.1016/j.eurpolymj.2016.10.030.

[5] Guo, K., Ren, Y., Han, G., Xie, T., Jiang, H. (2025). Hygrothermal aging and durability prediction of 3D-printed hybrid fiber composites with continuous carbon/Kevlar-fiber and short carbon-fiber, Eng Fail Anal, 167, p. 108958. DOI: 10.1016/j.engfailanal.2024.108958.

[6] Hachimi, T., Majid, F., Zekriti, N., Rhanim, R., Rhanim, H. (2024). Improvement of 3D printing polymer simulations considering converting G-code to Abaqus, The International Journal of Advanced Manufacturing Technology, 131(9), pp. 5193–5208. DOI: 10.1007/s00170-024-13300-9.

[7] Hachimi, T., Naboulsi, N., Majid, F., Rhanim, R., Mrani, I., Rhanim, H. (2021). Design and Manufacturing of a 3D printer filaments extruder, Procedia Structural Integrity, 33, pp. 907–916. DOI: 10.1016/j.prostr.2021.10.101.

[8] Jayaraman, R. (2019). 10 - Time-dependent damage evolution in unidirectional and multidirectional polymer composite laminates., In: Guedes, R.M. ed., Creep and Fatigue in Polymer Matrix Composites (Second Edition), Woodhead Publishing, pp. 303–321.

[9] Jia, Y., Ling, F., Qian, J., Chen, Q., Zhao, Z., Li, Y. (2023). Fast Damage-Healing of Rigid Photocuring 3D Printing Materials Capable of Directly Recycling in 3D Printing, ACS Macro Lett, 12(6), pp. 719–724.
[10] Koščo, T., Ďurka, R. (2022). Digital image correlation for accurate strain measurement on sharp notched specimens, Procedia Structural Integrity, 42, pp. 1600–1606.
[11] Lach, R., Schmidtke, A., Key, L.C., Langer, B., Grellmann, W. (2022). Fracture mechanics performance of 3D printed amorphous thermoplastic polymers at impact and quasi-static loading, Procedia Structural Integrity, 42, pp. 3–8. DOI: 10.1016/j.prostr.2022.11.002.
[12] Liu, W., Yang, X.J. (2013). Damage evolution with growing cyclic creep and life prediction of MDYB-3 PMMA, Fatigue Fract Eng Mater Struct, 36(6), pp. 483–491.
[13] Lutovinov, M., Halama, R., Papuga, J., Bartošák, M., Kuželka, J., Růžička, M. (2022). An Approximate Method for Calculating Elastic–Plastic Stress and Strain on Notched Specimens, Materials, 15(4), p. 1432.
[14] Majid, F., Elghorba, M. (2017). HDPE pipes failure analysis and damage modeling, Eng Fail Anal, 71, pp. 157–165. DOI: 10.1016/j.engfailanal.2016.10.002.
[15] Majid, F., Hachimi, T., Rhanim, H., Rhanim, R. (2023). Delamination effect on the mechanical behavior of 3D printed polymers, Frattura Ed Integrità Strutturale, 17(63), pp. 26–36.
[16] Manoj, I., Kumar Shah, A., Jain, A. (2024). Strength and failure assessments of 3D printed PLA single lap joints: Experimental and numerical analysis, Eng Fail Anal, 161, p. 108257. DOI: j.engfailanal.2024.108257.
[17] Mayén, J., Gallegos-Melgar, A.D.C., Pereyra, I., Poblano-Salas, C.A., Hernández-Hernández, M., Betancourt-Cantera, J.A., Mercado-Lemus, V.H., Monroy, M.D.A. (2022). Descriptive and inferential study of hardness, fatigue life, and crack propagation on PLA 3D-printed parts, Mater Today Commun, 32, p. 103948.
[18] Mobarak, M.H., Islam, M.A., Hossain, N., Al Mahmud, M.Z., Rayhan, M.T., Nishi, N.J., Chowdhury, M.A. (2023). Recent advances of additive manufacturing in implant fabrication – A review, Applied Surface Science Advances, 18, p. 100462. DOI: 10.1016/J.APSADV.2023.100462.
[19] Moetazedian, A., Gleadall, A., Mele, E., Silberschmidt, V. V. (2021). Damage in extrusion additive manufactured biomedical polymer: Effects of testing direction and environment during cyclic loading, J Mech Behav Biomed Mater, 118, p. 104397. DOI: https://doi.org/10.1016/j.jmbbm.2021.104397.
[20] Moetazedian, A., Gleadall, A., Mele, E., Silberschmidt, V. V. (2020). Damage in extrusion additive manufactured parts: effect of environment and cyclic loading, Procedia Structural Integrity, 28, pp. 452–457. DOI: 10.1016/j.prostr.2020.10.053.
[21] Monkova, K., Papadopoulou, S., Bouzouni, M., Toulfatzis, A., Pantazopoulos, G. (2024). The effect of 3D printing orientation on tensile behaviour and fracture mechanisms of Inconel 718, Eng Fail Anal, 166, p. 108920. DOI: 10.1016/j.engfailanal.2024.108920.
[22] Muna, I.I., Mieloszyk, M., Rimasauskiene, R., Maqsood, N., Rimasauskas, M. (2022). Thermal effects on mechanical strength of additive manufactured CFRP composites at stable and cyclic temperature, Polymers (Basel), 14(21), p. 4680.
[23] Naboulsi, N., Hachimi, T., Majid, F., Rhanim, R., Zekriti, N., Rhanim, H. (2021). Modeling and control of 3D filament extruder, Procedia Structural Integrity, 33, pp. 989–995. DOI: 10.1016/j.prostr.2021.10.109.
[24] Patel, P., Gohil, P. (2021). Role of additive manufacturing in medical application COVID-19 scenario: India case study, J Manuf Syst, 60, pp. 811–822. DOI: 10.1016/J.JMSY.2020.11.006.
[25] Penumakala, P.K., Santo, J., Thomas, A. (2020). A critical review on the fused deposition modeling of thermoplastic polymer composites, Compos B Eng, 201, p. 108336. DOI: 10.1016/j.compositesb.2020.108336.
[26] Picard, M., Mohanty, A.K., Misra, M. (2020). Recent advances in additive manufacturing of engineering thermoplastics: Challenges and opportunities, RSC Adv, 10(59), pp. 36058–36089. DOI: 10.1039/D0RA04857G.
[27] Rehman, M., Yanen, W., Mushtaq, R.T., Ishfaq, K., Zahoor, S., Ahmed, A., Kumar, M.S., Gueyee, T., Rahman, M.M., Sultana, J. (2023). Additive manufacturing for biomedical applications: a review on classification, energy consumption, and its appreciable role since COVID-19 pandemic, Progress in Additive Manufacturing, 8(5), pp. 1007–1041.
[28] Rejdali, H., Salhi, I., Hajjaji, A., Jay, J., Belhora, F. (2024). Effect of DMSO and Triacetin Solvents on Polyvinylidene Fluoride Polymorphs: Molecular Dynamics Simulations, Physica Status Solidi (a), 221(16), p. 2400207.
[29] Taoufik, H., Fatima, M., Hassan, R. (2023). Modeling of the fracture behavior of the 3D Printed polymers using XFEM, Procedia Structural Integrity, 47, pp. 711–722. DOI: 10.1016/j.prostr.2023.07.048.
[30] Vanaei, H.R., Shirinbayan, M., Vanaei, S., Fitoussi, J., Khelladi, S., Tcharkhtchi, A. (2021). Multi-scale damage analysis and fatigue behavior of PLA manufactured by fused deposition modeling (FDM), Rapid Prototyp J, 27(2), pp. 371–378. DOI: 10.1108/RPJ-11-2019-0300.
[31] Zekriti, N., Majid, F., Taoufik, H., Tounsi, Y., Rhanim, R., Mrani, I., Rhanim, H. (2023). Improvement of crack tip position estimation in DIC images by image processing methods, Frattura Ed Integrità Strutturale, 17(63), pp. 61–71.

[32] Zhang, D., Dong, Q. (2020). Fracturing and damage of 3D-printed materials with two intermittent fissures under compression, Materials, 13(7), p. 1607.
[33] Zhou, X., Feng, Y., Zhang, J., Shi, Y., Wang, L. (2020). Recent advances in additive manufacturing technology for bone tissue engineering scaffolds, International Journal of Advanced Manufacturing Technology, 108(11–12), pp. 3591–3606. DOI: 10.1007/S00170-020-05444-1.
[34] Zhu, L., Wang, G., Jia, Y., Wang, H., Wang, P., Li, D. (2023). Determination of the size effect on the tensile properties of miniaturized specimens, Materials Testing, 65(4), pp. 524–535.